ELECTRON LOADING

W. Weingarten
CERN, Geneva, Switzerland

1. INTRODUCTION

Superconducting r.f. cavities offer the possibility to sustain high electromagnetic fields without an excessive generation of heat. For electric surface fields of typically 10^7 V/m the accompanying wall losses amount to typically 10 W/m at 500 MHz. This low heat dissipation makes them extremely sensitive to losses which can be neglected in normal conducting cavities.

An often encountered mechanism of parasitic loss is electron loading. This term describes the generation of free electron currents which absorb energy from the cavity field and transfer this energy to the cavity wall. The power they liberate there is mainly transformed into heat. Already typical average currents of micro-ampères accelerated to typical energies of MeV can yield a heat dissipation of ~ 10 W/m, which is comparable to the r.f. wall losses.

The generation of electrons may be due to field emission, thermionic emission or secondary processes like secondary emission, electron back-scattering or photo-emission. Among these, field emission and secondary emission are mainly observed in superconducting cavities. Field emitted electrons are generated in regions of high electric fields and load the cavity because they can pick up high kinetic energies from the

electromagnetic field. Secondary electrons are generated in regions of low electric field and give rise to high currents due to a resonant effect. Thus, the electron loading of superconducting cavities is generally classified into two categories: non-resonant electron loading (NREL) for electrons originating in regions of high electric field and resonant electron loading (REL) or electron multipacting for electrons set free in regions of low electric field.

The body of knowledge up to 1980 on these two electron loading phenomena is presented at the Karlsruhe Workshop on R.F. Superconductivity by C. Lyneis: Electron loading - description and cures [1]. So I consider it sufficient to review new results obtained since then.

The main ideas presented at Karlsruhe are the following. With regard to NREL an intrinsic frequency dependence is stated, imposing strong electron loading on low frequency accelerating cavities and making high frequency cavities more favourable. Helium processing, i.e. operating the cavity beyond the level of start-up of NREL at a low helium partial pressure inside the cavity, is already known to be a technique for reducing NREL. Improved diagnostic methods [2] show that NREL is due to individual isolated electron emitters.

Concerning REL the understanding of one side electron multipacting at Stanford [3] and the advent of spherical cavities found free from one side electron multipacting after experimental investigations and a computational analysis at Genova [4] and Wuppertal [5] result in the start of an experimental program at CERN [6] to study spherical cavities at 500 MHz. At the Karlsruhe Workshop already first encouraging results on 500 MHz spherical cavities are presented, confirming that one side multipacting can be suppressed by a proper shape of the cavity. The question whether multicell spherical cavities have the same benefits is still unanswered. These results make all laboratories working in the field of high energy e^+e^- storage ring physics to adopt a rounded geometry.

Thus, since 1980, there is general agreement on REL to be overcome by a proper shaping of the cavity, and on NREL to become even more important at higher fields and to be far from reasonably well understood (in particular the apparent frequency dependence).

In my talk I will review in two chapters NREL and REL. The topics covered are:

(a) New experimental methods.
(b) What is the nature of the electron emitters?
(c) Is there a basic frequency dependence of NREL?
(d) Remedies against NREL.
(e) Is REL completely settled in spherical cavities?

2. NON-RESONANT ELECTRON LOADING

2.1 New experimental methods

Up to the Karlsruhe Workshop, the analysis of NREL is based on experimental information from integral quantities like the Q degradation, the X-ray intensity measured outside the cryostat, or the electron current picked up by an antenna in the cavity (fig. 1). Already at Karlsruhe measurements aiming at the study of individual emitters are reported [2] and since then exploited.

2.1.1 Studying individual electron emitters

A prerequisite of the investigation of individual electron emitters is a technique for measuring temperature (and X-ray) signals on the surface of the cavity with high spatial resolution. This requirement is met by the scanning resistor (and X-ray) system developed at CERN [6]. A calibration of the measured local temperature signal to the local power flux has become available [7]. That allows a calorimetric determination of the field emission currents. Another approach is the direct measurement of the field emitted current of single emitters with very high collection efficiency in cavities of a reentrant shape [8,9].

2.1.2. Broad area scanning of cavity surfaces

The first method is applied at CERN and has become common practice. The temperature profile (electron trajectory) due to impinging electrons is analyzed in order to extract:

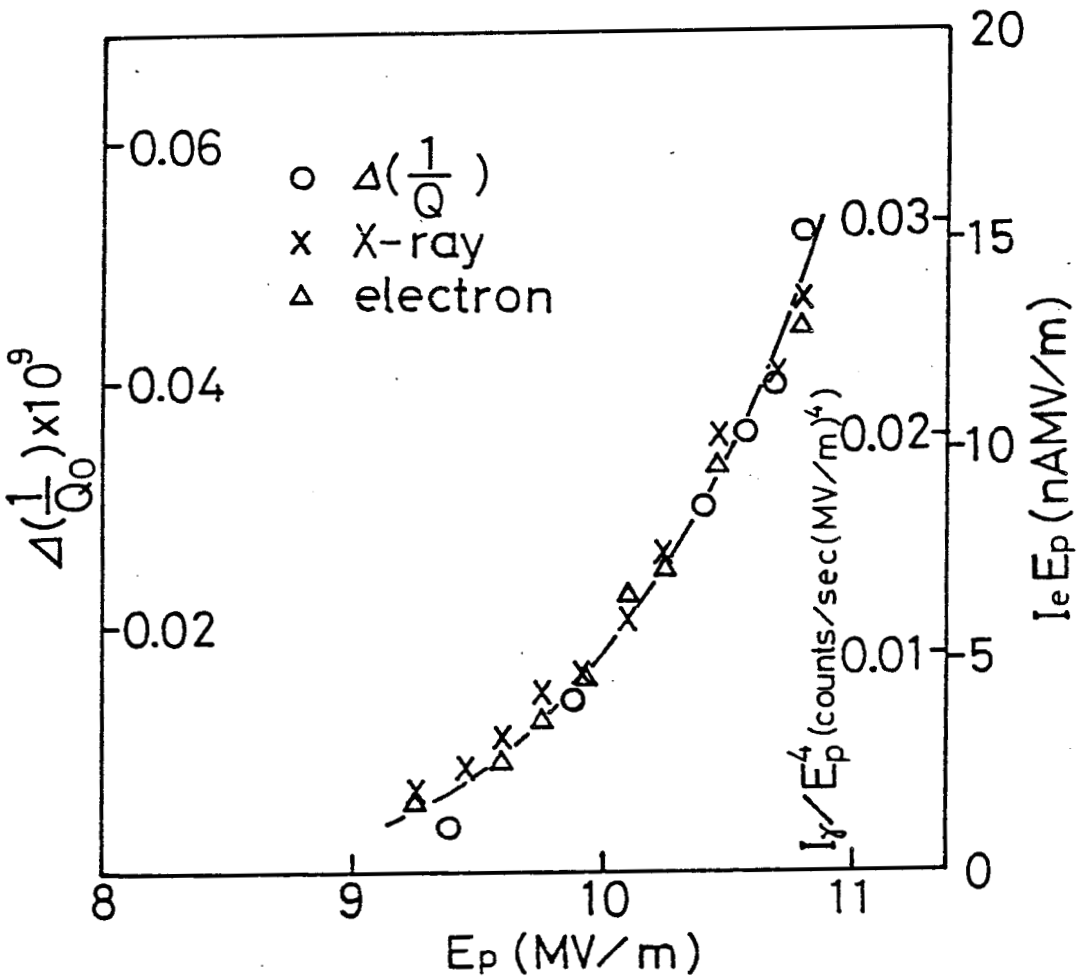

Fig. 1 Δ ($1/Q_o$), electron and X-ray intensity with increasing field (courtesy Y. Kojima)

- the location of a single emitter and the distribution of the emitters on the surface;
- intrinsic emitter features like the local field enhancement factor β, and the emitting area A.

For this purpose the computer codes which track the path of an electron in the electromagnetic field of a cavity are applied to correlate the measured power loss profile at a given accelerating field to the emitter location s_o, the emitting area A, and the field enhancement factor β as free parameters under the hypothesis of Fowler-Nordheim field emission. β is rather than a real field enhancement factor considered as a fit parameter which makes up for the uncertainty of the local electric field and work function to compensate the deviation of the measured current field relation from the Fowler-Nordheim current field relation [10]. In addition to that, attempts have been made to reinterprete β under a different hypothesis of electron emission (e.g. thermionic emission of hot electrons [11]). It turns out that the emitter location s_o is rather independent of the model for electron emission and may be determined with an accuracy of a few millimeters [6].

2.1.3 Measurements with reentrant cavities

The second method using reentrant cavities is pursued in Wuppertal and Karlsruhe. At Wuppertal [8] the experiment is directly linked with accelerator application, because the cavity is treated in the standard way (chemical polishing, high temperature annealing). Whenever an emitter is present on the reentrant cavity tip its current versus field relation is measured. The cavity (fig. 2) can be exited in different coaxial cavity modes at 0.5, 1.5, 2.5 and 3.5 GHz, which allows the study of an intrinsic frequency dependence of the r.f. field emission process itself.

At Karlsruhe [9], a tungsten field emission tip of well known shape (and consequently β) is introduced into a reentrant cavity in order to show the feasibility of an r.f. field emission source. This is of technical interest, because the electrons are already emitted in bunches at a well defined frequency. Also the question whether r.f. field emission follows the laws of d.c. field emission is studied. It is found out that the work function of tungsten, measured at microwave frequencies, is somewhat lower than that from d.c. measurements.

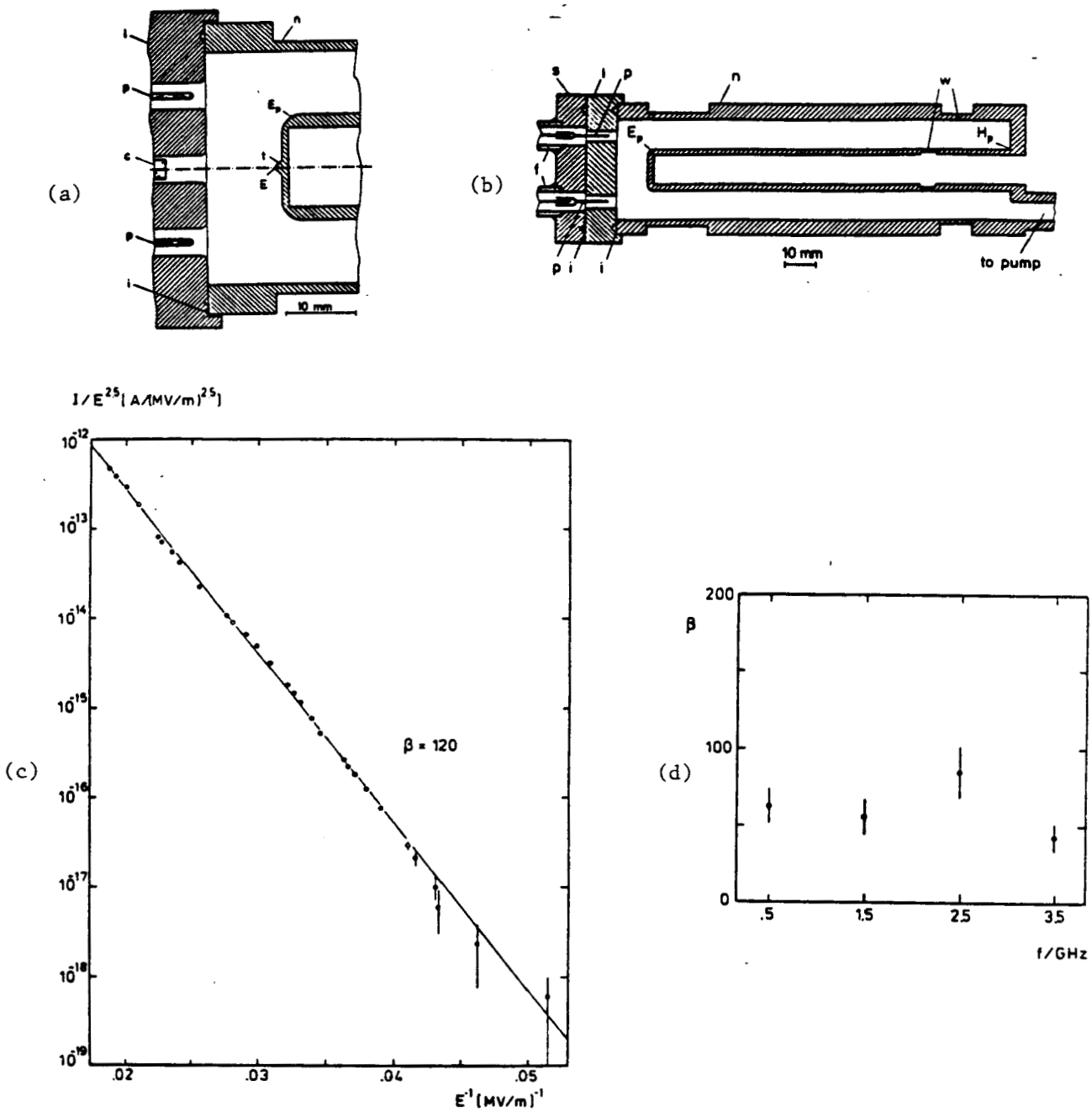

Fig. 2 Results from a multimode reeantrant cavity (from ref. [8]):

(a) Field emission geometry in the gap region
(b) Layout of reentrant cavity
(c) Fowler Nordheim plot
(d) Field enhancement factor versus frequency

In order to get more insight into the physical and chemical nature of electron sources, particles of different chemical composition are intentionally introduced in a superconducting 500 MHz cavity at CERN [12].

2.2 On the nature of electron emitters

2.2.1 Thermionic versus field emission

Broad area scanning on cavities is systematically performed at CERN on a vertically mounted cavity [13] and on two horizontally mounted cavities (c.f. also tables 1 and 2). Two alternative hypothesis are tested: thermionic emission, for which the emission current is independent of the r.f. electric field, and field emission, for which the emission current follows the r.f. electric field in a way described by the Fowler-Nordheim law with β as a free parameter.

A total of 19 electron trajectories are analyzed in the vertically mounted cavity, some of them at different accelerating fields. In no case the assumption of thermionic emission has given a reasonable fit. Therefore, it is concluded that cold cathode field emission is the dominating process. This is also found true for all electron trajectories analyzed in the horizontally mounted cavities. It is also in accordance with observations for the reentrant cavity experiment [8], where the current field relation follows a Fowler-Nordheim law over seven decades in current and about a factor of three in field (fig. 2). Thus, for the emission of the primary electrons there is no indication for another process than field emission.

2.2.2 Microparticles as electron emitters

Interesting results emerge from a correlation of the emitter location s_o to the treatment and mounting position of the cavity. Apart from one, all emitters are located at the bottom of the cavity in the region of maximum electric field at the iris rounding. During this series of measurements the cavity has intentionally undergone a change in the position for the chemical treatment (upside down), for the drying (vertical to horizontal), for the mounting (upside down), and for the attachment of the pumping tube (from above to from below). A clear preference of the emitter location to the bottom part of the cavity, when

it is mounted, is found, independent of its position during all other steps of the treatment. This is a strong support of the idea that microparticles (dust) or condensation products from residual gases are involved in the emission of electrons.

The idea of microparticles as electron emitters is in addition supported by other observations: the narrow width of e^- trajectories indicates pointlike sources. Detected sources are never visible at a later optical inspection. The density of sources is small (~ 1 on 10 cm^2 of cavity surface for $E \lesssim 10$ MV/m), which rules out grain boundaries, oxide inhomogeneities and microcracks.

Also influenced by these observations, a group for studying d.c. field emission is established at the University of Geneva. Up to now very similar results are found [14].

After plenty of experimental evidence is available for microparticles being electron sources, the question for their chemical composition arises. Experiments are under way at CERN, in which microparticles of different composition are intentionally introduced in microwave cavities. Carbon particles were already found to emit electrons [12].

2.2.3 Advantages of horizontal mounting

In recent measurements at CERN with horizontally mounted cavities (table 2) 16 emitters have been localized in an annular region of high electric surface fields $\lesssim 16$ MV/m (fig. 3(a)). The density of emitters is estimated to 1 on 25 cm^2 area, already somewhat lower than for the vertically mounted cavity.

For the series of measurements of a vertically mounted cavity [6], where no helium processing has been applied, the β from the current measurement amounts to 700 ± 100, the maximum field without any electron loading observed to 3.3 ± 0.3 MV/m. These figures can be considered as typical for vertically mounted cavities at 500 MHz after r.f. processing. Similar results are obtained at Karlsruhe [15]. In horizontally mounted cavities the electron loading is found to be reduced or not observable up to surface fields of 13 MV/m [16]. Typical β values are 480 ± 120, corresponding to threshold fields for the start-up of electron loading of

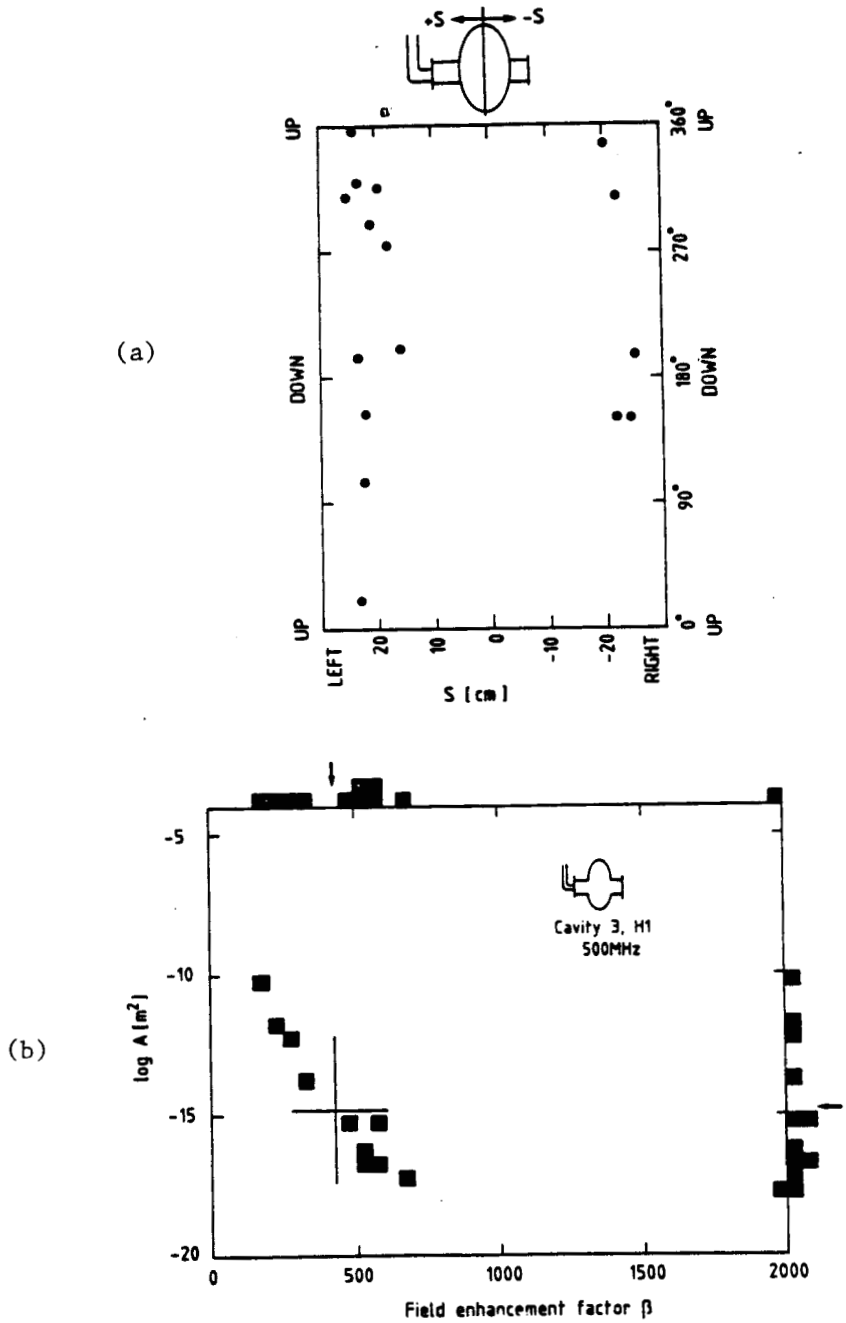

Fig. 3 Analysis of "e^- trajectories" from two horizontally mounted CERN 500 MHz cavities: (a) localization of emitters, (b) emitting area versus field enhancement factor (average and r.m.s. deviation are indicated).

4.8 MV/m. This result is due to a reduced probability of microparticles to be deposited in the regions of high electric field either during mounting or during operation.

This is also documented by recent results on a horizontally mounted cavity (table 1), which show that the emitters are distributed in a broader region in the vicinity of the iris (fig. 3(a)), and no longer on the iris rounding alone . As near the iris the electric surface field is steeply varying with position, emitters located away from the iris are exposed to a lower electric surface field. Thus on the average, the electron emission at a given accelerating field is also reduced. β is usually calculated from the current field relation assuming the emitter is located at the maximum surface electric field. It is therefore underestimated by the ratio of local to maximum surface electric field. Taking this into account the β values for the horizontally mounted cavities cover the same range as those for the vertically mounted cavities.

After the importance of the horizontal mounting position and the dust-free environment during the final stages of assembly has become evident (also including slow pumping down), the distribution of the emitter location in the horizontally mounted cavity does no longer show an up-down asymmetry (fig. 3(a)). This might be a hint on a second class of emitters, not being deposited onto, but buried in the material.

These three observations mentioned before, the point-like nature of the electron sources, their low density and the dependence of distribution and location of the electron sources on the mounting position of the cavity, support the hypothesis that they are microparticles collected and deposited during the final stages of mounting. The last observation indicates a second class of electron emitters attached to the bulk niobium itself.

2.2.4 Determination of the emitting area and field enhancement factor from cavity measurements

More information about A and β can be deducted from a detailed analysis of temperature maps of electron trajectories [17]. The power flux at a distinct location of the cavity is proportional to the product

of the current impinging there and the impact energy. As the power flux is measured and the impact energy is known from the electric field inside the cavity, the current can be determined. Since each position of electron impact corresponds to a r.f. phase of emission, the current versus phase relation at the moment of electron emission can be derived. In practice, measured and computed data are fitted with s_o, β and A as fit parameters. A current versus phase relation as in fig. 4(a) is expected and found (fig. 4(b)). From the peak current (~ 100 μA) and the Fowler-Nordheim peak current density for $\beta E \sim 6.10^9$ V/m (~ 10^{11} A/m^2) the emitting area A is determined to be ~ 10^{-15} m^2.

A and β are plotted for 11 different and characteristic emitters (table 2 and fig. 3(b)). An average area and an average β can be derived: log A [m^2] = -15 ± 2.5, β = 430 ± 170. The upper limit for the emitting area is $(1 \times 10^{-6}\text{m})^2$ the lower $(2 \times 10^{-9}\text{m})^2$, which is the range of dimensions for microparticles found as electron emitters in d.c. measurements [18]. The correlation between log A and β may be simulated by the very small dynamic range of the field emission current which can be detected using the calorimetric method.

2.3 On the frequency dependence of NREL

At the Karlsruhe Workshop experimental data on electron loading from measurements on velocity of light accelerating cavities are presented [1]. An empirical result is the decrease of β values with increasing frequency. This observation might find its explanation in either an intrinsic frequency dependence of the emission process itself or be a consequence of the larger gap size or area of low frequency cavities.

Experiments with a superconducting reentrant cavity [8] ruled out explicitly a frequency dependence of the emission process in the frequency range of four measured coaxial modes of this cavity (0.5 GHz < f < 3.5 GHz) (fig. 2(d)).

Computations of NREL to understand this apparent frequency dependence are performed at Cornell [19]. It has been found that predominantly the

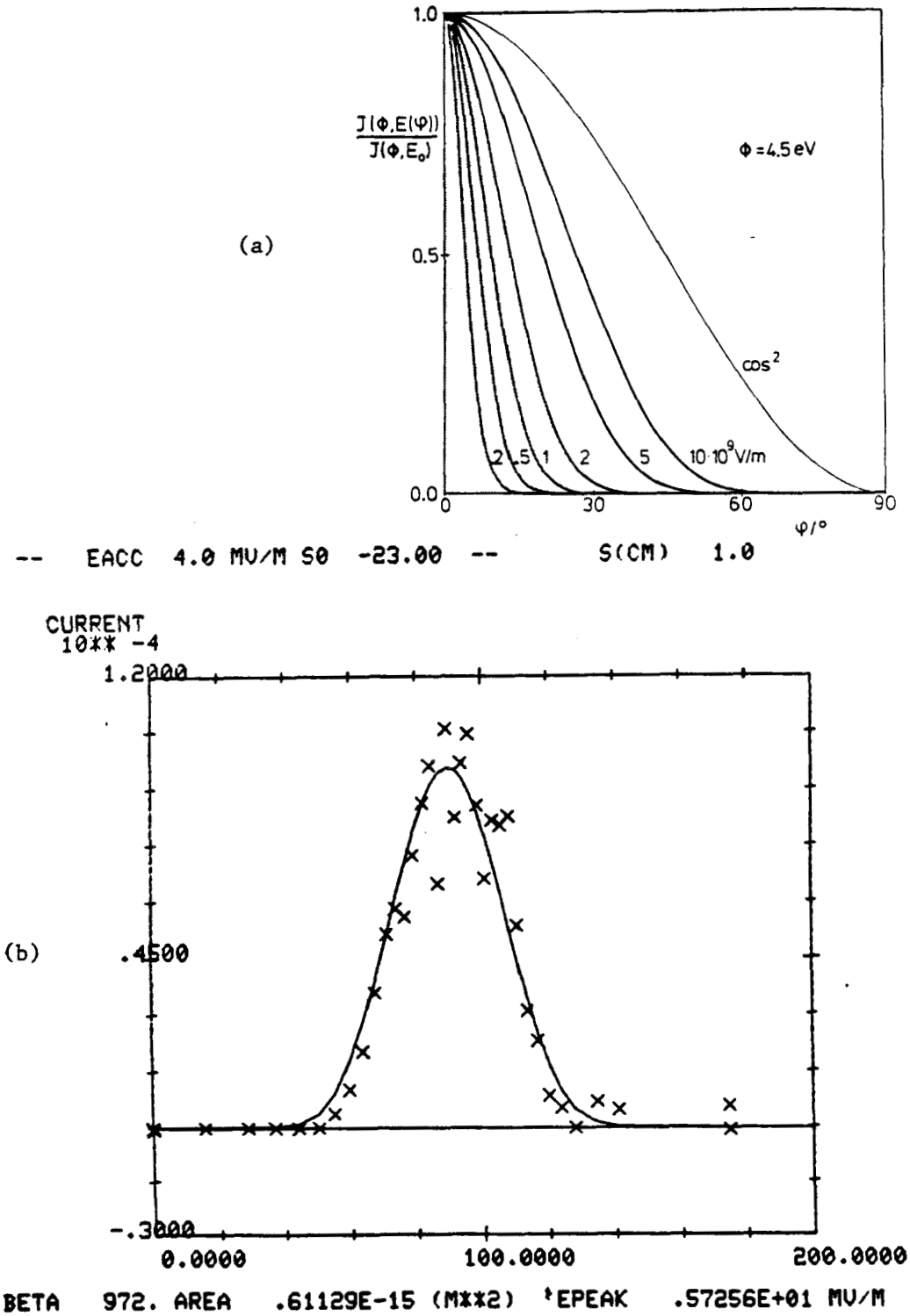

Fig. 4 Electron current versus r.f. phase: (a) calculated normalized Fowler-Nordheim current for a tungsten field emission tip with the local field as parameter (from ref. [9]); (b) measured electron current. The drawn line gives the best Fowler-Nordheim fit. The local electric field corresponds to 5.6 x 10^9 V/m.

Fowler-Nordheim current (the product of β value and local field) determines the total deposited power for unit accelerator length on an electron trajectory.

$$P\left[\frac{W}{cm}\right] \sim A\left[10^{-8}\ cm^2\right] \sqrt{\frac{1500}{f[MHz]}}\ 7.5 \times 10^4\ e^{-\frac{6.7 \times 10^4}{\beta E\ [MV/m]}}$$

If the field is limited by the maximum power per unit length which can be transferred to the helium bath, the frequency dependence of this power is by far too weak to explain the results presented at Karlsruhe.

A statistical model of field emission, which was originally proposed in ref. [20], might explain the apparent frequency dependence. It states that the emitters are uniformly distributed on the cavity surface with a low density. Under similar experimental conditions β values for three tests of L band cavities range from 314 to 377, those for six tests of S band cavities from 77 to 381. As one out of six S band cavity tests give a β value similar to those measured for L band cavities, and the area of an S band cavity is approximately 1/5 of the area of an L band cavity, these data support a statistical model.

To find more evidence for a statistical model, large data sets are needed. This has not yet been the case for storage ring cavities some years ago. However, since the Karlsruhe Workshop many measurements on storage ring cavities have been performed. Peak fields of 25 MV/m at 500 MHz [21] have been achieved recently (c.f. also table 1). This is far beyond the peak field according to the apparent Ep ~ f relation stated at Karlsruhe. It shows that with an improved treatment the probability for an emitter to occur can be reduced also in storage ring cavities of relatively low frequency. Whenever a large number of cavities of a particular frequency are measured, the β values reported do not vary markedly. β values measured for S band [22] and X band cavities [23] cover the same range as those for 500 MHz cavities. This supports a statistical model too.

2.4 Remedies of NREL

2.4.1 Helium processing

A powerful technique applied in all laboratories to reduce NREL is helium processing. Increases of fields by a factor of two and more are observed (fig. 5). It counteracts also efficiently against emitters which have withstood r.f. processing for many hours [16]. At Wuppertal, the accelerating field has been raised from 7 to 16 MV/m [22]. Also at Stony Brook NREL limits the maximum field to ~ 3 MV/m, after a period of r.f. processing, whereas helium processing increases the field by 1 MV/m. Then it tends to saturate [24]. Also at CERN, the field has been increased by a factor of 2 (fig. 5(b)), after nine hours of helium processing [12]. A saturation is also found (fig. 6(c)). It may be explained by the observation that the number of emitters increases with field (fig. 6(b)). As the helium processing is performed for a constant total electron loading current, the total sputtering rate remains also constant. Thus, the total amount of sputtered material per unit time is constant, too. As for low fields, however, there are fewer emitters present than for high fields, the amount of sputtered material per emitter and per unit time is higher, yielding a faster reduction of β value and a faster increase of the field. At high fields, the number of emitters is high, which results in a lower sputtering rate for an individual emitter and a slower progress.

At CERN [16], the disappearance of electron trajectories was documented by temperature mapping (fig. 7). The beneficial effects of helium processing are preserved after a warm up to room temperature, and also after the cavity has been slowly exposed to laboratory air at room temperature for some days.

Helium processing has first been systematically studied at Stanford [25]. An L band cavity was processed for 51 h which resulted in a reduction of β from 547 to 206. In the earlier stages of processing, β decreases by a factor 1/2 in 10 h. By sputter simulation calculations, it was found out that a monolayer (of a material which has the same sputter yield as niobium) was sputtered away in 50 to 500 s. The fast progress observed in the earlier stages of sputtering (c.f. also fig. 6(c))

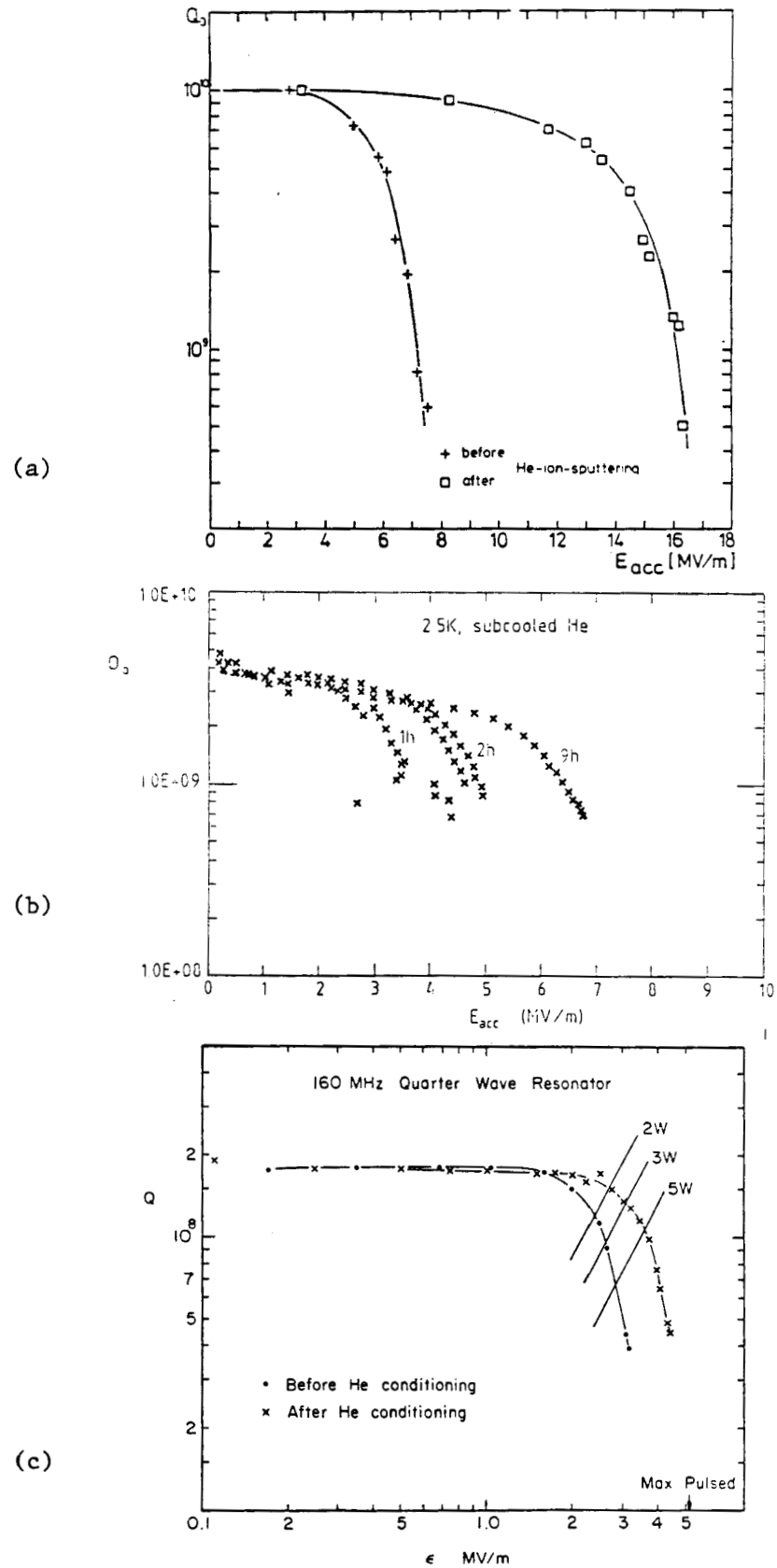

Fig. 5 **Field increase by helium processing: (a) S band [22], (b) 500 MHz [12] and (c) 160 MHz [24].**

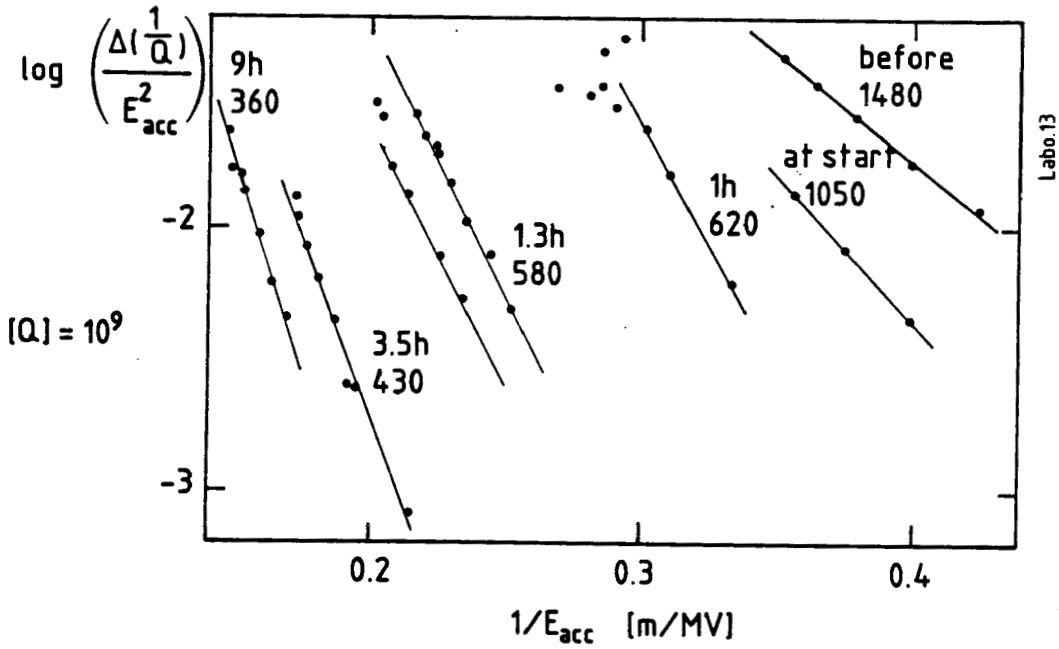

(a)

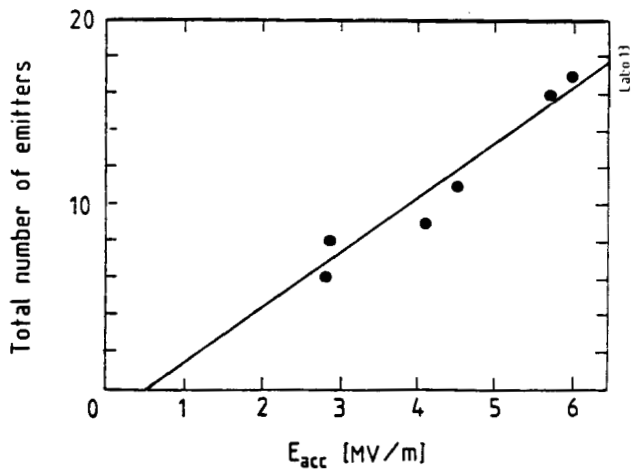

(b)

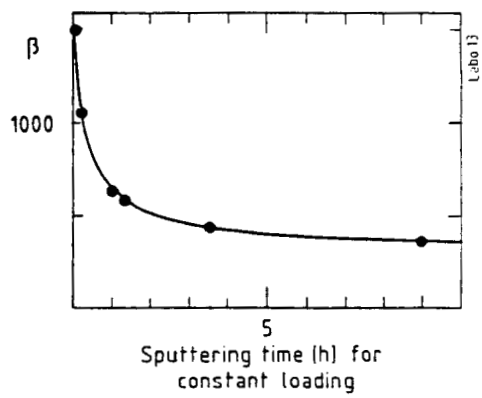

(c)

Fig. 6 Electron loading during field increase by helium processing (from ref. [12]: (a) Fowler-Nordheim plot from Q degradation (fig. 5(b)), (b) increase of number of emitters with field, including also those which were sputtered away and (c) decrease of β with time.

is therefore explained by the removal of a surface layer, which might have enhanced the emission by resonant tunnelling of electrons. The slower progress later on is explained by the removal of bulk material.

Also at CERN sputtering rates are computed for 500 MHz and the volume of the sputtered material is estimated [17]. Sputtered volumes were ~ $(1\ \mu m)^3$, emitting areas ~ $(1\ \mu m)^2$. A monolayer is sputtered in ~ 10 s. If one takes into account the different experimental parameters this rate has to be decreased by one order of magnitude for comparing it with the Stanford L band results. Then the sputtering rates agree on a sound basis.

The fair agreement between the cubic root of the sputtered volumes (0.3 to 0.5 μm) and the quadratic root of the emitting areas suggest the idea that a compact micro-particle or fragment of such a particle has induced the electron emission and is sputtered away, which is another support for the microparticle hypothesis for NREL. This also explains why the beneficial effect of helium processing continues after warm up and also after dust-free gas exposure.

2.4.2 Other methods under study

Very recently, high surface electric fields (25 MV/m) have been obtained at CERN (table 1) after an anodization to 100 V (~ 0.2 μm) and at Cornell [23]. NREL is found to be reduced. Even no sign of NREL is visible at Cornell up to surface fields of 22 MV/m after the cavity has been anodized to 200 V (0.4 μm). These results may support the idea that NREL decreases with the thickness of the anodized layer, which has already been found in d.c. field emission experiments by the Orsay Group [26].

At SLAC, pulsed high power r.f. processing at strongly coupled S band cavities has recently been applied [27]. When the field is increased, breakdowns occur, associated with a burst of X-rays (> 3 röntgen/h with less than 10^{-4} duty cycle), which decrease both in rate and intensity within minutes or faster. After such a breakdown the peak surface field is increased stepwise up to 68 MV/m. Helium processing subsequently applied does not improve the peak fields, which indicates that all the surface property related field emission has been processed away by peak field r.f. processing.

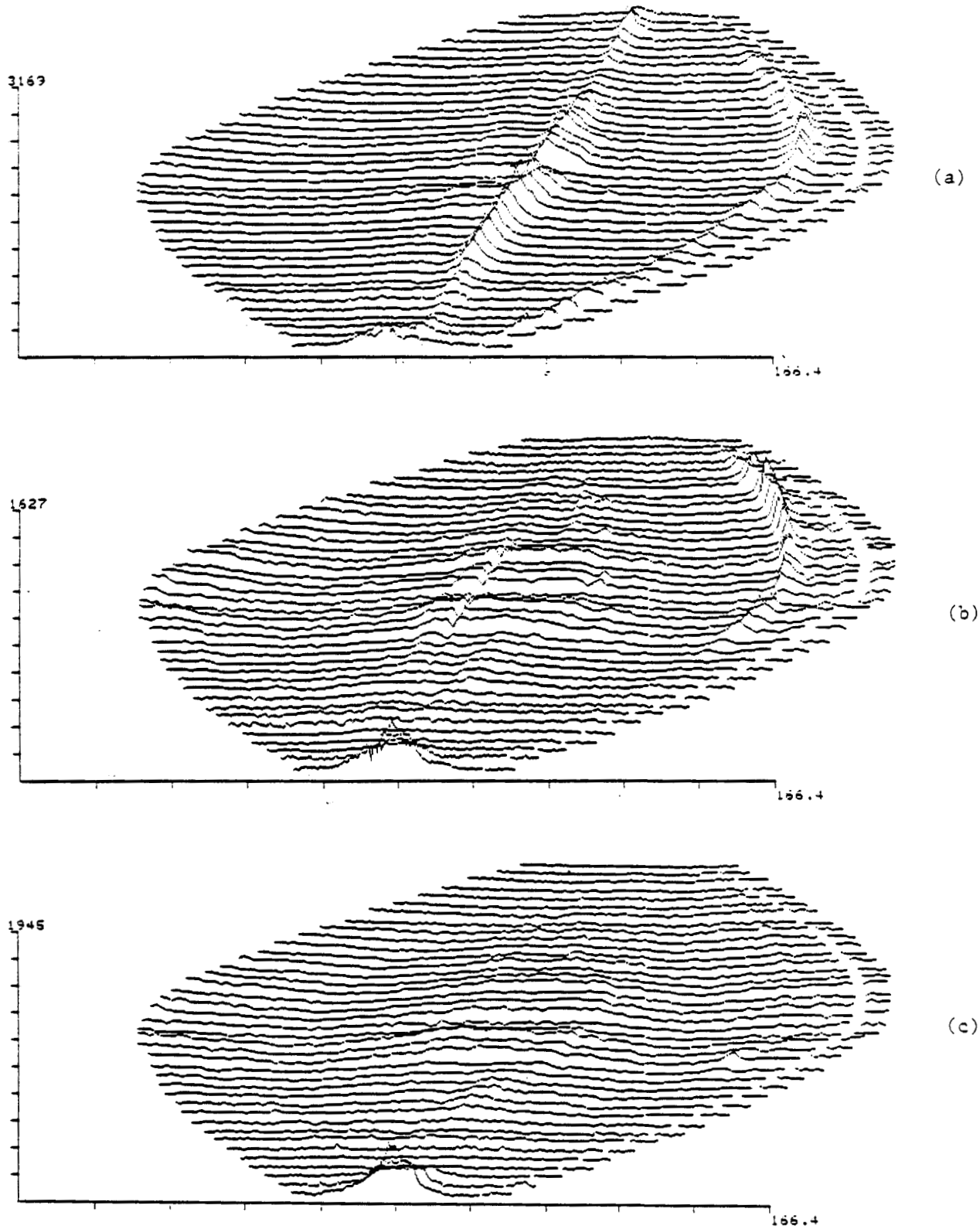

Fig. 7 Temperature map with "e^--trajectories": (a) before helium processing (E_{acc} = 6.7 MV/m), (b) during helium processing (E_{acc} = 6.7 MV/m) and (c) after helium processing (E_{acc} = 7.0 MV/m).

2.5 Conclusion

I conclude therefore, that there exists experimental support for the following assertions:

(a) NREL is caused by microparticles being either deposited on the cavity during the final stages of assembly and/or inherent to the material itself.

(b) The frequency dependence of NREL, stated at Karlsruhe, is explained by a homogeneous and rare event deposition of emitters per unit area. To have one emitter of high β value on a low frequency cavity surface is therefore more probable than to have the same emitter on a high frequency cavity surface of the same shape.

(c) Methods to reduce NREL are:

- avoiding dust deposition (slow pumping, horizontal mounting);
- helium processing;
- r.f. processing (in particular high power pulsed r.f. processing for heavily coupled cavities);
- possibly anodization.

3. RESONANT ELECTRON LOADING - MULTIPACTING

3.1 Is REL completely settled in spherical cavities?

Since the Karlsruhe Workshop spherically (or elliptically) shaped cavities prevail in all laboratories where superconducting electron accelerator structures are developed. The original idea, which make them superior to other cavity geometries, is the suppression of one side multipacting. In particular, storage ring cavities operated at relatively low frequencies allow a crucial test to multipacting. In the majority of experiments multipacting is absent in single-cell and multicell spherical cavities (operated in the fundamental accelerating mode) [6,16,28-31]. Only occasionaly, e.g. after an insufficiently clean surface treatment or temporarily during field increase, multipacting is observed. In Cornell [32], in a cavity subjected to an acetone rinsing with drops of oil added, multipacting levels are found. In the first test of the 350 MHz cavity, the field of which is limited by a thermal quench at 4.7 MV/m caused by a

defect in a weld, only slight indications of losses due to REL are observed. They can be elimitated by r.f. processing [33].

Any deviation from the rotational symmetry makes these cavities more sensitive to multipacting. At CERN, single-cell cavities with coupling ports at the equator for the fundamental mode power input and the higher order mode damping show indications of multipacting without affecting the maximum field obtained [34]. This observation is no surprise, since one side multipacting favourably establishes itself at surface regions with nearly constant and low electric surface field. Any hole near the equator weakens the steep decrease of surface electric field towards the equator, by which a field configuration favouring one side multipacting is generated. Temperature signals associated with electron currents due to multipacting are observed in such cavities around the higher order mode coupling port. Also in a 5-cell cavity, assembled from five single-cell cavities of that shape, multipacting near the higher order mode coupling port was detected [35]. The field levels at which multipacting occurs are 4.5, 3.0, 2.5 and 1.4 MV/m. In these tests the quality of the rinsing water has not yet been optimal. Then, its purity is controlled in a new installation. A field of 5 MV/m can be reached without any indication of a resonance due to electrons [21]. The absence of multipacting is an indication for the crucial importance of the last rinsing step for the surface properties like the secondary emission coefficient.

3.2 Two side multipacting in spherically shaped cavities

3.2.1 Experimental observations

A new observation is made in two 500 MHz cavities produced from niobium sheet material with improved thermal conductivity (λ = 28 W/m/K), and in two 350 MHz cavities. A first series of measurements with these cavities is given in table 1. Higher fields than ever before can be achieved in the 500 MHz cavities which is attributed to the higher thermal conductivity of the material [36]. That makes the observation of new electron loading phenomena possible.

In this test series a common feature is revealed. Between 8 and 10 MV/m (500 MHz) these cavities are affected by REL. This leads to a thermal quench and can only be surmounted by both r.f. and helium processing of some hours (test 2 and 3, cavity H1, table 1).

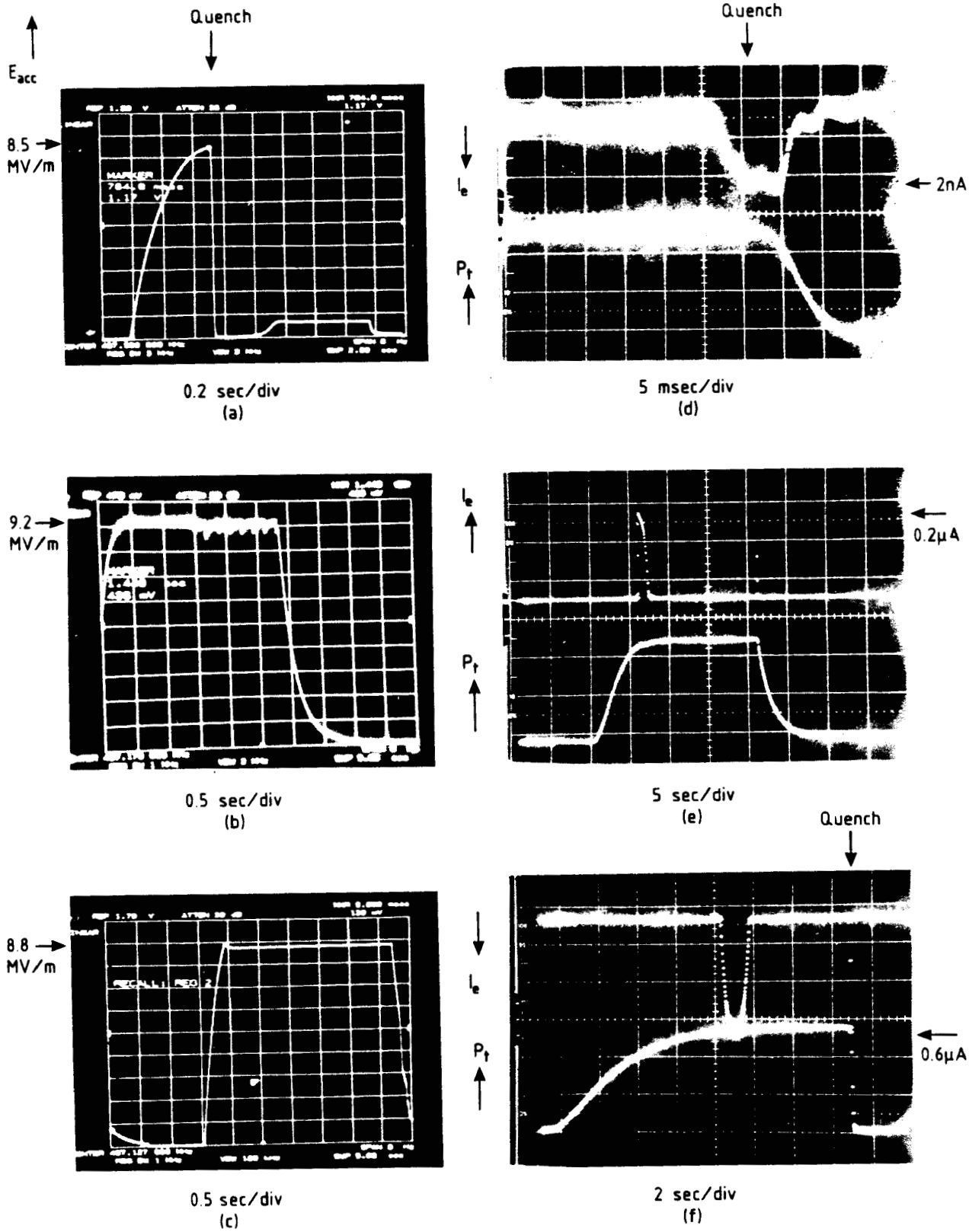

Fig. 8 Diagnosing electron multipacting: (a) accelerating field showing quench, (b) limitation, (c) limitation and levels; (d) correlation of electron current I_e with transmitted power P_t in quench, (e) and (f) after the level is passed.

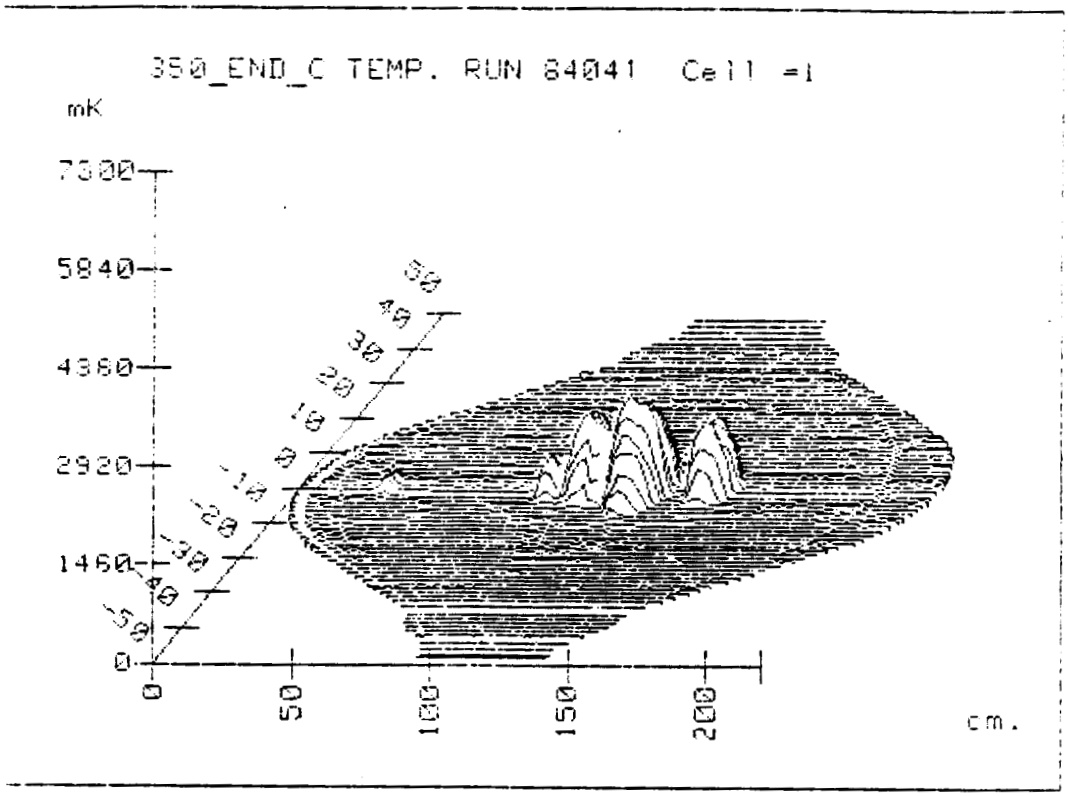

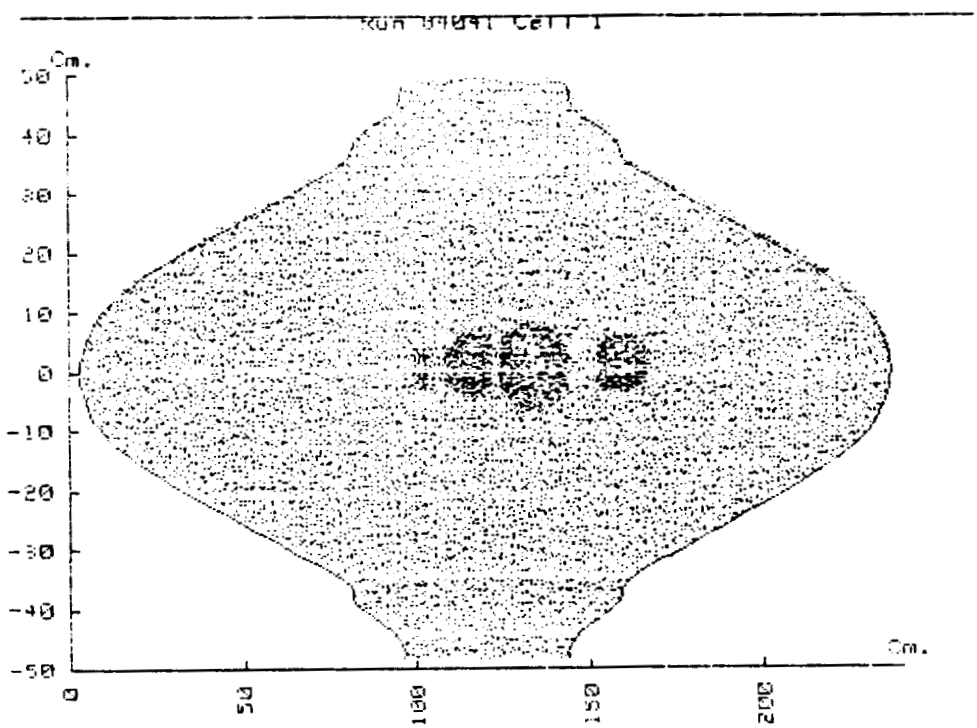

Fig. 9 **Temperature maps of 350 MHz cavity during quench at 5.6 MV/m**

This electron resonance is associated with well known features for multipacting (fig. 8): flat top of transmitted signal, correlated with an electron current picked up by an antenna, bursts of electrons and X-rays in the quench, kinks in the transmitted signal due to a Q degradation at a certain field level and correlated with a current signal. The possibility to increase the field slightly in the presence of a higher mode frequency injected into the cavity uncovers the resonant nature of the quench. Whenever the cavity field is limited by a quench at 8 MV/m < E_{acc} < 10 MV/m, the corresponding temperature signal is found at the equator. Two 350 MHz cavities show very similar features at 5.4 < E_{acc} < 5.6 MV/m, which correspond to the field level of REL at 500 MHz, scaled with frequency. Also this level cannot be passed. By temperature mapping it is documented that at a field level just above the quench field several regions, all very near to each other, show a temperature signal (fig. 9). This has never been observed for a thermal quench due to a hot spot and indicates the resonant character of the losses. Thus, experimental evidence for multipacting at the equator in cavities of spherical shape is available.

3.2.2 Results from multipacting simulation calculations

In order to understand this phenomenon, electron multipacting is simulated, based on a routine for computing electron tracks in the r.f. field of a cavity [37]. Following the successful explanation of observed multipacting levels by mere electron kinematics [5], only secondary electron emission is considered. The electrons start with 2 eV perpendicular to the surface, the most probable energy for secondary electrons [38].

The results are the following (fig. 10(a)):

(a) Resonant electron trajectories are found at 9.5 ± 3.5, 3.17, 1.9, 1.36, 1.06, ... MV/m, corresponding to a magnetic field

$$B_n \text{ [mT]} = 72 \text{ f [GHz]}/(2n-1), \quad n = 1, 2, \ldots$$

(b) Flight times between impacts are half integers of an r.f. period (i.e. half a period for the uppermost resonance).

(c) The impact energy for the uppermost resonance (at 9.5 MV/m) depends linearly on the starting energy. For 2 eV it amounts to 30 eV.

(d) The impact energy for the lower resonances is approximately equal to the starting energy (2 eV starting energy corresponds to 2 eV impact energy).

A typical example of an electron track for the upper most resonance is shown in fig. 10(b).

Thus, from the correspondence between the experimental data and the computer simulation it is concluded that the observed resonance is due to two-side multipacting at the equator.

3.2.3 Can this two side multipacting be passed

It is astonishing, that such a relatively low impact energy yields a secondary emission coefficient high enough to give multiplication. Looking at table 1, however, a correlation between the quench location and that part of the cavity which is at the bottom during the drying process, always performed in a horizontal position, is disclosed. In particular, in cavity 2, which was mounted vertically, such that no preferential up/down asymmetry with regard to the equator is present during operation, the quench location is also found at that region. It is therefore suspected that drying residuals affect the secondary emission coefficient in such a way that already for the most probable impact energy of 30 eV electron multiplication may occur. That the field threshold has been passed through twice reveals that this impact energy is very near to the lower threshold energy E_1, for which the secondary coefficient δ exceeds 1. Measurements performed at CERN [39] show that for proper cleaned niobium surfaces (gas discharge cleaning and baking) E_1 exceeds 60 (fig. 11). Only for samples kept at air for hours, δ ranges from 38 to 80. Thus, there are indications that the threshold should be overcome by an improved surface preparation.

3.3 Conclusion

I conclude therefore, that in storage ring cavities of the rounded shape REL is absent up to a field of ~ 60 mT • f [GHz]. This is true for single-cell and multicell cavities in the π accelerating mode. Cavities with coupling ports at the equator and/or non properly cleaned surfaces show a tendency to enhanced REL. Above this field REL is

observed at the equator, preferentially where a high secondary coefficient is expected. This level can occasionally be passed through. These are indications that this REL is linked with impact energies very near to the lower crossover energy E_1 of oxidized niobium. To shed light onto this observation, measurements of the secondary emission coefficient for niobium samples treated in the same way as a cavity (wet surface dried during air exposure) have to be performed.

4. CONCLUSION AND OUTLOOK

By clean and dust-free preparation methods, horizontal mounting, and processing techniques, the electric surface field above which NREL sets in is raised up to more than 25 MV/m also at a low frequency like 500 MHz. Evidence is growing for NREL being induced by particles of the submicron diameter range. The often observed decrease of NREL with frequency may be explained by a rare event homogeneous spatial distribution of emitters of a distinct β value. Processing techniques (helium and/or r.f. processing) allow a reduction of NREL, but tend to saturate. High power pulsed r.f. processing has not yet been extensively studied and may offer an effective reduction of NREL.

Two-side electron multipacting at the equator of spherically shaped cavities is discovered. It is found predominantly at regions suspected of contaminations. It is correlated to a surface with a lower crossover energy for the secondary coefficient $E_1 \simeq 30$ eV, typical of niobium exposed to air and smaller than that for clean niobium. Improved cleaning methods might reduce the danger of encountering a field limitation by that two-side multipacting.

Acknowledgements

I am very grateful to H. Lengeler and H. Piel for their help and comments in the course of preparing this talk. Indispensable were also the information and written comments of P. Kneisel, H. Padamsee and R. Sundelin of Cornell, D. Proch of DESY, U. Klein of Interatom, J. Halbritter of Karlsruhe, Y. Kojima of KEK, I. Campisi and D. Farkas of SLAC, A. Schwettman of Stanford HEPL, M. Brennan of Stony Brook, and G. Müller of Wuppertal.

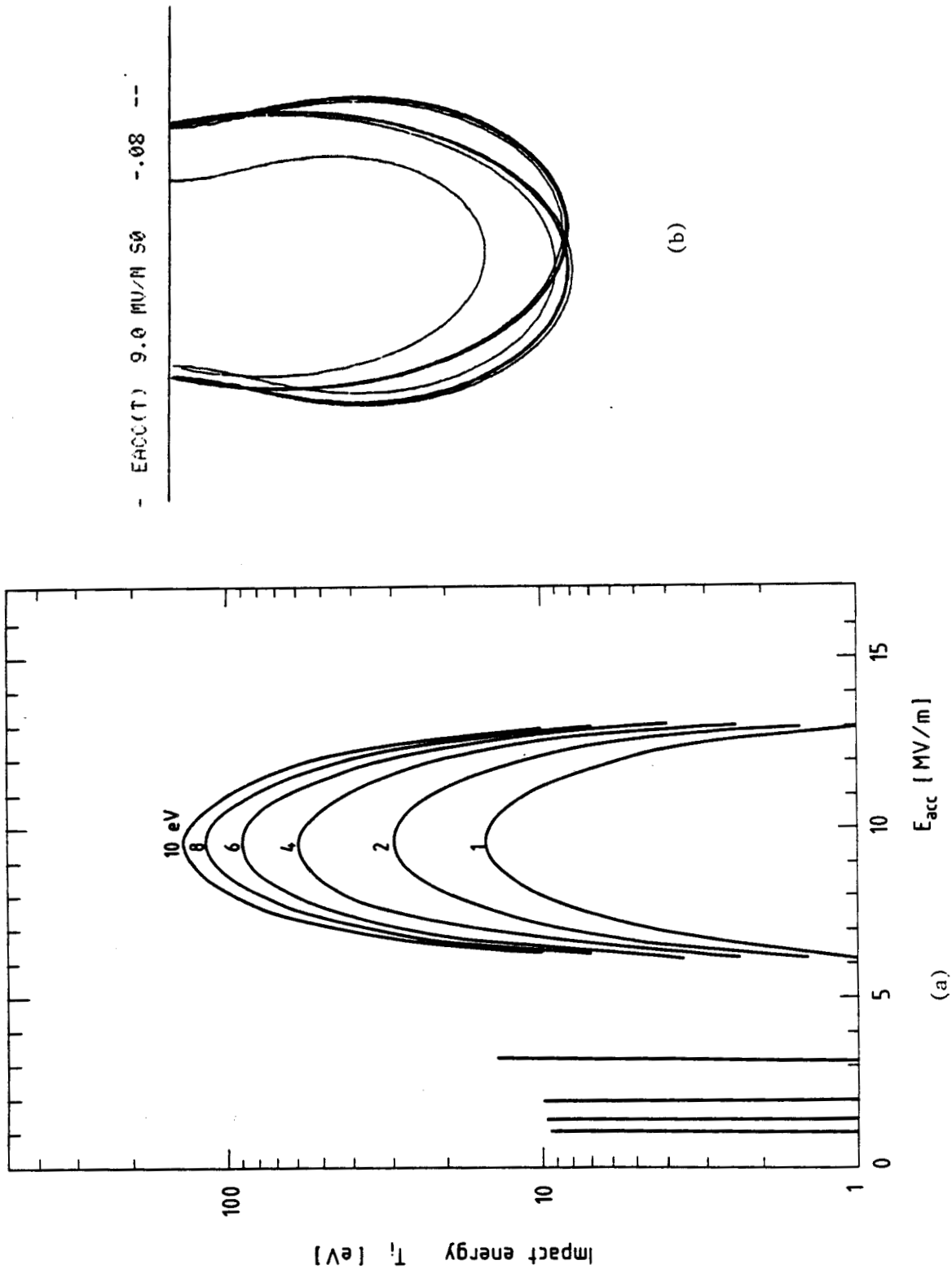

Fig. 10 Two side electron multipacting at the equator of a 500 MHz spherical cavity: (a) impact energy versus accelerating field with the starting energy of the secondary electrons as parameter, (b) typical electron track for the first order. The distance of points of impact is ~ 1 mm.

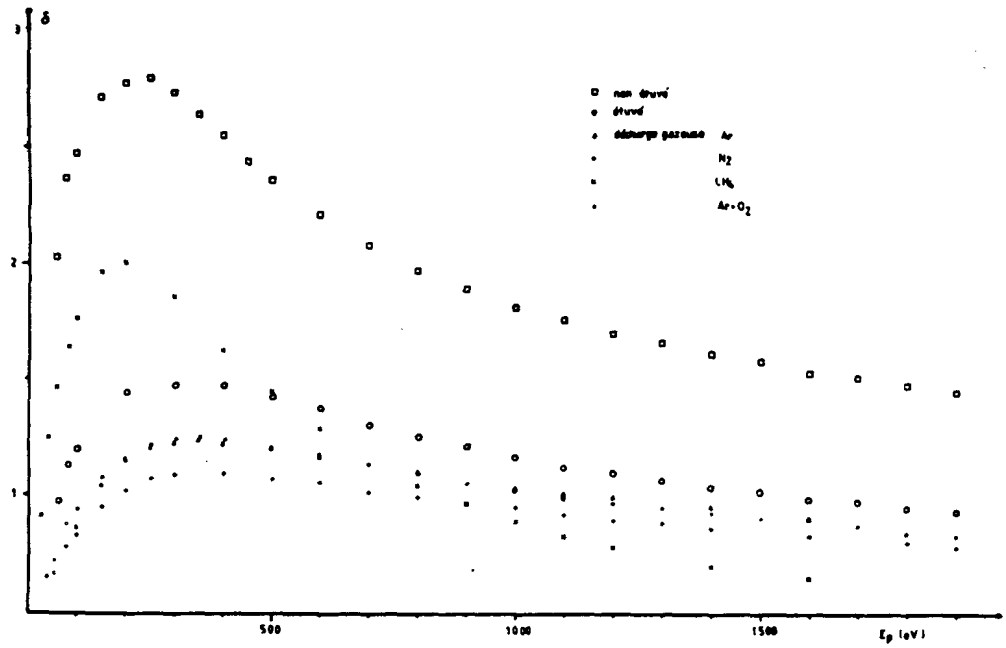

TRAIT.	δ_{100eV}	δ_{1000eV} (eV)	E_1 (eV)	E_2 (eV)	E_{max}	δ_{max}
RECEPTION	2.47	1.8	-	-	250	2.79
ETUVE	1.2	1.17	60	1550	300	1.48
DECHARGE GAZEUSE AZOTE						
Après dech.	0.83	.94	150	750	400	1.09
94h. N_2	1.01	1.03	100	1100	400	1.23
réétuvé	0.9	.99	150	950	300	1.23
48 h. air	1.07	1.13	70	1450	350	1.42
réétuvé	1.07	1.09	90	1300	300	1.37
DECHARGE GAZEUSE ARGON						
Après dech.	0.87	.98	115	980	300	1.25
8h. air	1.5	1.4	38	-	300	1.86
réétuvé	1.03	1.05	90	1150	300	1.31
DECHARGE GAZEUSE METHANE						
Après dech.	1.75	.9	140	850	200	2
DECHARGE GAZEUSE ARGON+OXYGENE						
Après dech.	1.03	.94	120	1100	350	1.25
66h. N_2	.99	1.08	103	1250	350	1.32
réétuvé	.96	1.07	105	1250	350	1.31
66 h. Air	1.09	1.16	80	1570	350	1.44
réétuvé	1	1.1	100	1350	350	1.35

Fig. 11 Secondary emission coefficient for Nb and different treatments (from [39])

TABLE 1

Recent cavity measurements at CERN showing e^- multipacting [21]

Cavity frequency (thermal conductivity) mounting position	Treatment	E_{acc}^{max} [MV/m]	Quench location and cause of quench
H1 500 MHz (λ = 28 W/m/K) horizontal	1 Standard [6] He processing	9.0	Eq. 175°, e^- multipacting
	2 Anodization He processing	13.0	near iris, hot spot
	3 De-anodization He processing	12.0	near iris, quench induced by NREL
	4 Local EP[(a)] He processing	9.4	eq. 180°, e^- multipacting
	5 Intentional production of phosphates[(a)]	8.4	eq., different positions, e^- multipacting
H2 500 MHz (28 W/m/K) vertical	1 Standard He processing	9.6	eq., different positions, e^- multipacting
350 MHz (10W/m/K) horizontal	1 Standard	4.7	eq. 40°, defect at weld
	2 Local repair [16] standard	5.4	e.q., different positions, defect or e^- multipacting
350 MHz (10 W/m/K) horizontal	1 Standard	5.4	eq., different positions, 180° finally, e^- multipacting
	2 Local repair anodization	5.6	eq., different positions, preferentially 180°, e^- multipacting

Eq. 180°: Equator (180°) corresponds to the cavity bottom during drying
Local EP: Electropolishing of local area of cavity

(a) D. Bloess, Chemistry and surface treatments, this Workshop.

TABLE 2

Analysis of "electron trajectories" in 500 MHz cavities(*)

No.	E_{acc} [MV/m]	E_{loc} [MV/m]	s_o [cm]	α [degrees]	I_p [μA]	β	$A^{1/2}$ [μm]	Remarks
1	6.7	11.7	23.3	313	35	330	0.140	b
2	6.7	11.6	23.1	192	120	280	1.000	d
3	6.7	13.0	24.0	306	30	245	1.300	d
4	8.0	12.8	22.0	147	75	-	-	a
5	8.3	6.6	15.7	198	400	1980	0.002	b
6	8.6	10.8	19.4	312	28	465	0.020	a
7	8.7	11.4	-20.0	345	14	540	0.005	a
8	9.0	9.8	17.8	273	100	580	0.020	b
9	3.7	6.7	23.5	18	1000	-	-	b
10	8.1	12.0	-21.5	153	350	-	-	b
11	8.1	14.8	24.1	357	200	-	-	b
12	8.7	13.9	-22.0	312	28	530	0.003	a
13	8.7	12.1	21.0	291	45	680	0.003	a
14	8.6	15.7	-23.9	195	60	170	8.000	a
15	9.1	14.6	22.5	105	140	560	0.005	b
16	8.1	15.7	-24.0	147	-	-	-	a

E_{acc}: accelerating field;
E_{loc}: local field at emitter location;
s_o: emitter location, latitude (equator: $s_o = 0$ [6]);
α: emitter location, meridian;
I_p: peak current at field maximum;
β: field enhancement factor;
A: emitting area;
b,d,a: before, during, after He processing.

(*) No. 1 to 3 are observed in "cavity 3" in ref. [16]; No. 4 to 16 are observed in "cavity H1", table 1.

REFERENCES

[1] C.M. Lyneis, Electron loading, Proceedings of the Workshop on RF Superconductivity, Karlsruhe, KfK 3019 (1980) 119.

[2] H. Piel, Diagnostic methods of superconducting cavities and identification of phenomena, Proceedings of the Workschop on RF Superconductivity, Karlsruhe, KfK 3019 (1980) 85.

[3] C.M. Lyneis, H.A. Schwettman and J.P. Turneaure, Elimination of electron multipacting in superconducting structures for electron accelerators, Appl. Phys. Lett. 31 (1977) 541.

[4] V. Lagomarsino, G. Manuzio, R. Parodi and P. Vaccarone, Measurements on niobium superconducting C-band cavities for linear accelerator applications, IEEE Trans. Mag. MAG-15 (1979) 25.

[5] U. Klein and D. Proch, Multipacting in superconducting r.f. structures, Proc. of the Conf. on Future Possibilities of Electron Accelerators, Charlottesville USA (1979).

[6] Ph. Bernard et al., Experiments with the CERN superconducting 500 MHz cavity, Nucl. Instr. & Meth. (1981) 257.

[7] R. Romijn, W. Weingarten and H. Piel, Calibration of the scanning thermometer resistor system for a superconducting accelerating cavity, IEEE Trans. Mag. MAG-19 (1983) 1318.

[8] U. Klein and J.P. Turneaure, Field emission in superconducting RF. cavities, IEEE Trans. Mag. MAG-19 (1983) 1330.

[9] H. Hübner, First results of a microwave field emission cathode, Optik 64 (1983) 113.

[10] J. Halbritter, On electron emission phemonena from oxidized metal surfaces, their application to electron loading in Nb high frequency cavities, KfK-Ext. 3/78-1 (1978).

[11] R.V. Latham, Prebreakdown electron emission, Proc. of the 10th Int. Symp. on Discharges and Electrical Insulation in Vacuum (1982) 3.

[12] C. Athwal and W. Weingarten, Carbon particle induced electron loading in a superconducting cavity, CERN/EF/RF 84-7 (1984).

[13] H. Lengeler, Diagnostics for superconducting r.f. cavities, IEEE Nucl. Sci. NS-28 (1981) 3217.

[14] Ø. Fischer, this Workshop.

[15] Sh. Noguchi, Y. Kojima and J. Halbritter, Measurements of a superconducting 500 MHz Nb cavity in the TM_{010} mode, Nucl. Instr. & Meth. 179 (1981) 205.

[16] Ph. Bernard et al., New results with superconducting 500 MHz cavities at CERN, Nucl. Instr. & Meth. 206 (1983) 47.

REFERENCES (Cont'd)

[17] J. Tückmantel and W. Weingarten, On electron loading in superconducting accelerating cavities, CERN/EF/RF 82-6.

[18] Ø. Fischer and R. Latham, private communication.

[19] H. Padamsee and R. Kahn, private communication.

[20] C. Lyneis, Y. Kojima, J.P. Turneaure, Nguyen Tuong Viet, Electron loading in L nd S band superconducting niobium cavities, IEEE Trans. Nucl. Sci. NS-20 (1973) 101.

[21] C. Benvenuti et al., RF superconductivity at CERN, new results, CERN/EF/RF 84-3 (1984) and H. Lengeler, this workshop.

[22] G. Müller and H. Piel, private communication.

[23] H. Padamsee, private communication.

[24] M. Brennan, private communication.

[25] H.A. Schwettman, J.P. Turneaure and R.F. Waites, Evidence for surface-state-enhanced field emission in r.f. superconducting cavities, J. Appl.Phys. 45 (1974) 914.

[26] G. Sayag, Nguyen Tuong Viet, H. Bergeret and A. Septier, Field emission from oxidized niobium electrodes at 295 and 4.2 K, J. Phys. E10 (1977) 176.

[27] I.E. Campisi and Z.D. Farkas, High gradient, pulsed operation of superconducting niobium cavities, SLAC/AP-16, February 1984, and this Workshop.

[28] P. Kneisel, R. Vincon and J. Halbritter, First results on elliptically shaped cavities, Nucl. Instr. & Meth. 188 (1981) 669.

[29] Y. Kojima, T. Furuya and T. Nakazato, Recent results on 500 MHz superconducting cavities at KEK, Jpn. Journ. Appl. Phys. 21 (1982) L86.

[30] P. Fernandez, V. Lagomarsino, G. Manuzio, R. Parodi and R. Vaccarone, C-band superconducting structure for a e^- linac, IEEE Trans. Mag. MAG-19 (1983) 1334.

[31] U. Klein, D. Proch and H. Lengeler, Report WU B 80-16, University of Wuppertal (1980).

[32] P. Kneisel, private communication.

[33] P. Bernard et al., First results on a superconducting 350 MHz cavity at CERN, CERN/EF/RF 83-6 (1983).

[34] P. Bernard et al., Results of the tests of the single cell 500 MHz accelerating cavities for the PETRA 5-cell cavity, CERN/EF/RF 82-9.

REFERENCES (Cont'd)

[35] P. Bernard et al., Status report of the superconducting 5-cell acceleration structure at CERN, IEEE Trans. Nucl. Sci. NS-30 (1983) 3342.

[36] H. Lengeler, W. Weingarten, G. Müller and H. Piel, Superconducting niobium cavities of improved thermal conductivity, Proc. Appl. Superconductivity Conference, San Diego, CA, USA (1984) (to be published in IEEE Trans. Mag.).

[37] J. Tückmantel, private communication.

[38] O. Hachenberg and W. Brauer, Secondary electron emission from solids, Advances in Electronics and Electron Phycics, Volume XI, Academic Press, New York and London (1959), 413.

[39] N. Hilleret, Influence de traitements par décharge gazeuse sur l'émission électronique du niobium, Note technique CERN, LEP/VA/nh (1984).